



Design, synthesis and biological evaluation of edaravone derivatives bearing the *N*-benzyl pyridinium moiety as multifunctional anti-Alzheimer's agents

Luke S. Zondagh, Sarel F. Malan  and Jacques Joubert 

Pharmaceutical Chemistry, School of Pharmacy, University of the Western Cape, Bellville, South Africa

ABSTRACT

A series of multi-target directed edaravone derivatives bearing *N*-benzyl pyridinium moieties were designed and synthesised. Edaravone is a potent antioxidant with significant neuroprotective effects and *N*-benzyl pyridinium has previously exhibited positive results as part of a dual-site binding, peripheral anionic site (PAS) and catalytic anionic site (CAS), acetylcholinesterase (AChE) inhibitor. The designed edaravone-*N*-benzyl pyridinium hybrid compounds were docked within the AChE active site. The results indicated interactions with conserved amino acids (Trp279 in PAS and Trp84 in CAS), suggesting good dual-site inhibitory activity. Significant *in vitro* AChE inhibitory activities were observed for selected compounds (IC₅₀: 1.2–4.6 μM) with limited butyrylcholinesterase inhibitory activity (IC₅₀'s >160 μM), indicating excellent selectivity towards AChE (SI: 46 – >278). The compounds also showed considerable antioxidant ability, similar to edaravone. *In silico* studies indicated that these compounds should cross the blood–brain barrier, making them promising lead molecules in the development of anti-Alzheimer's agents.

ARTICLE HISTORY

Received 5 June 2020
Revised 15 July 2020
Accepted 18 July 2020

KEYWORDS

Alzheimer's disease;
edaravone; *N*-benzyl
pyridinium; cholinesterase;
oxidative stress



1. Introduction


Alzheimer's disease (AD) is a progressive neurodegenerative disorder that is mainly prevalent in the older population (>65 years of age)^{1–3}. Approximately fifty million people are diagnosed with dementia, with AD accounting for 60–70% of these cases⁴. The disease can be characterised by an array of symptoms which include; memory loss, cognitive impairment, behavioural and psychiatric abnormalities³. Due to the complex and multifactorial nature of AD, the exact aetiology of the disease is unknown. Multiple pathways and hypotheses have been indicated in the pathology of the disease such as the Aβ cascade-, cholinergic- and the oxidative stress hypotheses^{1,3,5}.

Senile plaques are considered a pathological hallmark of AD. The primary constituent of these senile plaques is Aβ and are believed to play a central role in the pathogenesis of the disease^{6,7}. The amyloid cascade hypothesis suggests that one of the main driving forces behind AD development is the buildup and deposition of Aβ peptide aggregation within the brain^{8,9}. Recently, it was discovered that the amyloid precursor protein (APP) gene undergoes mutations that induce an increase in Aβ formation. The APP mutations are situated near the sites where proteases, β and γ-secretase, cleave the APP. These mutations result in the favouring of the Aβ_{1–40} and Aβ_{1–42} peptide fragment formation^{7,8,10}. Aβ_{1–40} and Aβ_{1–42} are more inclined to self-aggregate to form amyloid beta fibrils. With the persistent imbalance of the production and clearance of the Aβ fragments, the consequential result is the genesis of insoluble senile plaques. These senile plaques result in the blockage of parenchymal spaces between neurons in the brain leading to eventual neuronal cell death^{8,9}.

The cholinergic hypothesis describes that the hydrolysis of the neurotransmitter acetylcholine (ACh) by cholinesterases, acetylcholinesterase (AChE) and butyrylcholinesterase (BuChE), leads to a drastic decrease in ACh levels. The loss of cholinergic transmission due to the decreased levels of ACh has been correlated with loss of memory and cognitive ability¹¹. AChE is the predominant enzyme that hydrolyse ACh in the healthy brain¹². The AChE enzyme contains a pocket with two binding sites, the catalytic anionic site (CAS) and peripheral anionic site (PAS). Interactions with both these sites are crucial for the inhibition of AChE activity and potential neuroprotective effects¹³. The PAS possesses a non-cholinergic role that through protein–protein interactions, bind to and promotes the formation and deposition of insoluble Aβ fibrils leading to neurotoxicity. Recent studies have shown that the inhibition in the PAS did not only improve the memory in a transgenic APP/PS1 murine model, but also significantly stemmed the amount of Aβ plaques in the brain^{14–16}.

Reactive oxygen species (ROS) are known to play a significant role in the progression of neurodegenerative disorders such as AD^{17–19}. The most significant ROS include hydroxyl radicals, superoxide anions and peroxyl radicals¹⁹. As ROS begins to accumulate and antioxidant levels begin to reduce, detrimental effects in the brain begin to occur. This process is further increased with aging^{17,19}. The brain is especially susceptible to the neurotoxic effects of ROS due to its high demand for oxygen as well as the large amounts of peroxide susceptible lipid cells¹⁸. ROS have also been observed to cause disruptions in neuronal cell integrity and to modify and inactivate several proteins that are important for glucose metabolism and ATP synthesis resulting in mitochondrial dysfunction^{10,18}. The occurrence of the neurotoxic effects of ROS in the development of AD, coupled with the presence of Aβ,

CONTACT Jacques Joubert  jjoubert@uwc.ac.za  School of Pharmacy, University of the Western Cape, Private Bag X17, Bellville, 7535, South Africa

 Supplemental data for this article is available online at [here](https://doi.org/10.1080/14756366.2020.1801673).

© 2020 The Author(s). Published by Informa UK Limited, trading as Taylor & Francis Group.

This is an Open Access article distributed under the terms of the Creative Commons Attribution License (<http://creativecommons.org/licenses/by/4.0/>), which permits unrestricted use, distribution, and reproduction in any medium, provided the original work is properly cited.

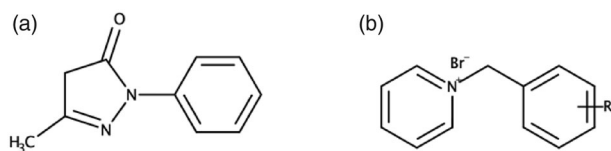


Figure 1. The two moieties combined to synthesise the novel MTDLs in this study. (a) Edaravone. (b) R-substituted *N*-benzyl pyridinium.

supports the role of oxidative stress in the pathogenesis of AD^{18,20,21}. Several lines of evidence have revealed a connection between oxidative stress and A β formation^{10,19,22}. A β exhibits the ability to enhance the formation of ROS and *vice versa*^{22,23}. A β produces ROS through the promotion of oxidative modification and inhibition of important transmembrane transports systems within the neuronal and glial cells, A β -induced lipid peroxidation and protein oxidation^{22,24,25}. In addition, ROS also stimulate the enhanced activity of proteases, β and γ -secretase, which increases the formation of A β_{1-40} and A β_{1-42} ²³.

At present, there are no therapeutic agents that are able to reverse, halt or slow the progression of the disease and the current options are only able to treat AD symptomatically^{2,11,26-28}. All of these treatments follow the much researched “one-molecule–one-target” drug discovery approach with minimal success. Therefore, more researchers are exploring the development of multi-target directed ligands (MTDL)²⁶. MTDLs are conceived from the molecular hybridisation of various pharmacophoric moieties from recognised bioactive compounds. The MTDLs are designed to interact with multiple targets involved in the multifactorial pathogenesis of AD. The rational decision to combine these pharmacophores results in greater selectivity for the targets of AD, leads to fewer side effects and potentially improves the compounds’ neuroprotective abilities^{29,30}.

Edaravone (Figure 1(a)) is a potent free radical scavenger used to treat acute cerebral infarction in Japan³¹. In addition, edaravone has also exhibited beneficial neuroprotective effects in amyotrophic lateral sclerosis (ALS) and Parkinson’s disease animal models³². Edaravone’s neuroprotective effects are believed to be caused by its ability to scavenge ROS. The decrease in ROS levels in turn reduces oxidative stress and oxidative damage to neuronal cells^{33,34}. In previous studies, edaravone has demonstrated the ability to attenuate A β -induced oxidative stress and neurotoxicity, inhibit A β aggregation, disaggregate preformed A β fibrils and attenuate downstream pathologies including tau-hyperphosphorylation, neuroinflammation and neuronal cell loss^{31,35}.

In search for potentially potent and selective AChE inhibitors, benzyl pyridinium salts have been extensively researched (Figure 1(b))³⁶⁻³⁹ and *N*-benzyl pyridinium moieties have demonstrated excellent activity against AChE. Previous research has found that the best AChE inhibitory activity is reached when the *N*-benzyl pyridinium moiety is bound to another privileged molecule, using the MTDL strategy, to form a dual-site (PAS and CAS) binding compound^{37,38}. Substitutions, e.g. halogens and methyl groups, at various positions on the benzyl group of the moiety has demonstrated improved AChE inhibitory activity compared to an unsubstituted benzyl ring^{36,40}.

Thus, we describe here the docking, synthesis and biological evaluation of new edaravone-*N*-benzyl pyridinium hybrid compounds (Figure 2). These compounds are expected to exhibit strong dual-site AChE inhibitory activities and significant antioxidant capacity, which could lead to promising MTDL neuroprotective effects.

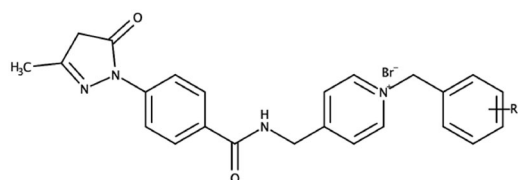


Figure 2. Edaravone-*N*-benzyl pyridinium hybrid compounds designed and evaluated in this study. R = H, Br, F, Cl, or CH₃.

2. Materials and methods

2.1. Chemistry

All the reagents used to synthesise the desired compounds were acquired from Sigma-Aldrich® or Industrial Analytical (Pty) Ltd. All the reagents were used without further purification. Solvents used in the synthesis and purification of the compounds were obtained from a variety of commercial sources. Thin-layer chromatography (TLC) was used to monitor all reactions and was carried out on 0.20 mm thick aluminium silica gel sheets (TLC silica gel 60 F245 Merck KGaA). Visualisation of the samples was achieved using UV light (254 nm and 366 nm) and iodine vapours. Mobile phases were prepared on a volume-to-volume basis. Infra-red spectra were acquired using a Perkin Elmer Spectrum 400 spectrometer. The IR spectrometer was equipped with a diamond attenuated total reflectance (ATR) attachment. The spectra were then acquired from PerkinElmer, Inc. Spectrum version 10.5.4 IR software. The MS spectra of the compounds were acquired from a Waters SYNAPT G2 high resolution mass spectrometer. The melting points of the samples were acquired using a Lasec Melting Point SMP 10 apparatus and capillary tubes. Proton (¹H) and carbon (¹³C) spectra were acquired using a Bruker Avance IIIHD Nanobay 400 MHz instrument that is equipped with a 5 mm BBO probe. Tetramethylsilane (TMS) was used as the internal standard and deuterated dimethyl sulfoxide (DMSO-d₆) as the deuterated solvent. Chemical shifts (δ) and coupling constants (*J*) were reported in parts per million (ppm) and hertz (Hz) respectively. The internal standard (δ = 0 ppm) and DMSO-d₆ (δ = 2.5 ppm) were used as the reference peaks. The multiplicities of the respective signals were indicated using the following abbreviations: s – singlet, d – doublet, t – triplet, m – multiplet. The atom numbering of the target compounds used for ¹H NMR data are depicted on each respective compound found in the [supplementary data](#).

2.1.1. Synthesis of 4-(3-Methyl-5-oxo-4H-pyrazol-1-yl)-*N*-(pyridine-4-ylmethyl)benzamide (3)

The 4-(aminomethyl)pyridine moiety was conjugated to the carboxylic group of **1** via HATU activation chemistry. One equiv. edaravone-COOH (**1**) and four equiv. of *N,N*-diisopropylethylamine (DIPEA) was stirred at room temperature for 20 min. Thereafter, the carboxylic acid of **1** was activated using the HATU activation agent in a 1 equiv.:1.2 equiv. ratio in an appropriate quantity of dimethylformamide (DMF). The mixture was stirred at room temperature for 1 h and monitored using TLC (3 ethanol: 2 ethyl acetate: 4 diethyl ether). Once the reaction was complete, 4-(aminomethyl) pyridine (**2**) was added to the mixture and stirred under reflux at 40–50 °C for 1 h and monitored using TLC. Once the reaction was complete, toluene was added to the mixture in a ratio of 3 equiv. toluene: 1 equiv. DMF. The reaction was then rotary evaporated until just off dry. The mixture was left to precipitate out overnight in a refrigerator. Finally, the precipitate was filtered and washed with distilled water. The precipitate was

placed in a vacuum oven and allowed to dry rendering the desired compound **3**.

Physical data: Yield: 72.52%; light pink solid; mp: 234 °C; Rf: 0.45; ¹H NMR: (400 MHz, DMSO-d₆), δ_H: 9.10–9.13 (t, 1H, *J* = 5.60, 5.83, 11.43 Hz, H—12), 8.50–8.51 (d, 2H, *J* = 5.88 Hz, H—16, 17), 7.95–7.98 (d, 2H, *J* = 8.68 Hz, H—6, 10), 7.85–7.87 (d, 2H, *J* = 8.64, H—7, 9), 7.30–7.32 (d, 2H, *J* = 5.76 Hz, H—15, 18), 4–4.9–4.51 (s, 2H, H—13), 2.13 (s, 3H, H—1); ¹³C NMR: (400 MHz, DMSO-d₆): 166.36, 149.98, 149.15, 128.66, 122.62, 120.10, 42.21, 14.70; IR: (FT-IR, cm⁻¹): 3217, 3035, 1713, 1637; MS: (HR-ESI⁺), [M + H⁺], *m/z*: calcd.: 309.1273, found: 309.1347.

2.1.2. General procedure for the synthesis of compounds **5a–l**

Compound **3** (1 equiv.) and 1.3 equiv. of the respective substituted benzyl bromide derivative (**4**) were dissolved and stirred under reflux, at 40–50 °C, in 5–6 ml of DMF. The compounds were monitored using TLC (3 ethanol: 2 ethyl acetate: 4 diethyl ether) for 4–6 h. Once the reaction was complete, 3 equiv. toluene: 1 equiv. DMF was added. The mixture was then rotary evaporated to dryness. Thereafter, 20 ml of diethyl ether was added to the dried mixture. The mixture was then left to precipitate out overnight in a refrigerator. Thereafter, if solid, the precipitate was filtered off and washed with diethyl ether. If the precipitate exhibited a waxy/oily appearance the mixture was diluted in a minimal amount of ethanol and transferred into a polytop. Finally, the precipitate or waxy/oily substance was dried, rendering the desired compounds **5a–l**.

2.1.2.1. 1-Benzyl-4-([4-(3-methyl-5-oxo-4H-pyrazol-1-yl)phenyl]foramido)methylpyridin-1-ium bromide (5a). Physical data: Yield: 95.29%; light grey solid; mp: 225 °C; ¹H NMR: (400 MHz, DMSO-d₆), δ_H: 9.33–9.36 (t, 1H, *J* = 5.60, 5.72, 11.32 Hz, H—12), 9.11–9.12 (d, 2H, *J* = 6.32 Hz, H—16, 17), 8.06–8.07 (d, 2H, *J* = 6.24 Hz, H—15, 18), 7.97–7.99 (d, 2H, *J* = 8.60 Hz, H—6, 10), 7.87–7.89 (d, 2H, *J* = 8.64 Hz, H—7, 9), 7.43–7.53 (m, 5H, H—21, 22, 23, 24, 25), 5.83 (s, 2H, H—19), 4.72–4.74 (d, 2H, *J* = 5.28 Hz, H—13), 2.13 (s, 3H, H—1); ¹³C NMR: (400 MHz, DMSO-d₆): 166.68, 162.79, 160.74, 159.84, 144.80, 134.87, 129.83, 129.72, 129.59, 129.23, 128.96, 128.84, 126.55, 119.36, 117.36, 63.14, 42.80, 17.19; IR: (FT-IR, cm⁻¹): 3184, 3034, 1717, 1639; MS: (HR-ESI⁺), [M-Br]⁺, *m/z*: calcd.: 399.1815, found: 399.1820.

2.1.2.2. 1-[(2-Fluorophenyl)methyl]-4-([4-(3-methyl-5-oxo-4H-pyrazol-1-yl)phenyl]foramido)methylpyridin-1-ium bromide (5b). Physical data: Yield: 97.17%; black solid; mp: 191 °C; ¹H NMR: (400 MHz, DMSO-d₆), δ_H: 9.33–9.36 (t, 1H, *J* = 5.72, 5.83, 11.55 Hz, H—12), 9.03–9.04 (d, 2H, *J* = 6.44 Hz, H—16, 17), 8.06–8.08 (d, 2H, *J* = 6.52 Hz, H—15, 18), 7.87–8.00 (m, 4H, H—6, 7, 9, 10), 7.58–7.62 (t, 1H, *J* = 7.68, 7.56, 15.24, Hz, H—22), 7.51–7.55 (m, 1H, H—23), 7.34–7.35 (d, 1H, *J* = 1.88 Hz, H—24), 7.30–7.32 (d, 1H, *J* = 7.96 Hz, H—25), 5.93 (s, 2H, H—19), 4.74–4.75 (d, 2H, *J* = 5.40 Hz, H—13), 2.14 (s, 3H, H—1); ¹³C NMR: (400 MHz, DMSO-d₆): 166.69, 162.78, 162.20, 161.08, 145.01, 132.65, 132.57, 131.96, 128.83, 126.53, 125.81, 125.78, 121.87, 121.72, 117.37, 116.62, 116.41, 57.83, 42.84; IR: (FT-IR, cm⁻¹): 3201, 3034, 1717, 1638; MS: (HR-ESI⁺), [M-Br]⁺, *m/z*: calcd.: 417.1721, found: 417.1719.

2.1.2.3. 1-[(3-Fluorophenyl)methyl]-4-([4-(3-methyl-5-oxo-4H-pyrazol-1-yl)phenyl]foramido)methylpyridin-1-ium bromide (5c). Physical data: Yield: 98.48%; brown solid; mp: 220 °C; ¹H NMR: (400 MHz, DMSO-d₆), δ_H: 9.33–9.36 (t, 1H, *J* = 5.60, 5.83,

11.43 Hz, H—12), 9.11–9.13 (d, 2H, *J* = 6.64 Hz, H—16, 17), 8.07–8.08 (d, 2H, *J* = 6.56 Hz, H—15, 18), 7.87–8.00 (m, 4H, H—6, 7, 9, 10), 7.48–7.54 (m, 1H, H—23), 7.45–7.48 (d, 1H, *J* = 10.2, H—21), 7.37–7.39 (d, 1H, *J* = 7.72 Hz, H—25), 7.26–7.31 (m, 1H, H—24), 5.85 (s, 2H, H—19), 4.73–4.75 (d, 2H, *J* = 5.32, H—13), 2.14 (s, 3H, H—1); ¹³C NMR: (400 MHz, DMSO-d₆): 166.68, 163.88, 161.44, 160.89, 144.89, 137.26, 137.18, 131.91, 131.82, 128.84, 126.58, 125.48, 125.45, 119.39, 117.36, 116.87, 116.47, 62.34, 42.82, 17.18; IR: (FT-IR, cm⁻¹): 3201, 3036, 1716, 1638; MS: (HR-ESI⁺), [M-Br]⁺, *m/z*: calcd.: 417.1721, found: 417.1732.

2.1.2.4. 1-[(4-Fluorophenyl)methyl]-4-([4-(3-methyl-5-oxo-4H-pyrazol-1-yl)phenyl]foramido)methylpyridin-1-ium bromide (5d). Physical data: Yield: 87.13%; light grey solid; mp: 215 °C; ¹H NMR: (400 MHz, DMSO-d₆), δ_H: 9.32–9.35 (t, 1H, *J* = 5.60, 5.80, 11.43 Hz, H—12), 9.09–9.10 (d, 2H, *J* = 6.64 Hz, H—16, 17), 8.05–8.07 (d, 2H, *J* = 6.48 Hz, H—15, 18), 7.87–7.99 (m, 4H, H—6, 7, 9, 10), 7.61–7.64 (m, 2H, H—22, 25), 7.28–7.32 (t, 2H, *J* = 8.80, 17.60 Hz, H—21, 25), 5.81 (s, 2H, H—19), 4.72–4.73 (d, 2H, *J* = 5.44 Hz, H—13), 2.13 (s, 3H, H—1); ¹³C NMR: (400 MHz, DMSO-d₆): 166.67, 164.27, 161.82, 160.76, 144.72, 131.93, 131.85, 131.09, 131.06, 128.94, 128.83, 126.55, 117.36, 116.74, 116.53, 62.29, 42.81, 17.19; IR: (FT-IR, cm⁻¹): 3201, 3036, 1716, 1638; MS: (HR-ESI⁺), [M-Br]⁺, *m/z*: calcd.: 417.1721, found: 417.1729.

2.1.2.5. 1-[(2-Chlorophenyl)methyl]-4-([4-(3-methyl-5-oxo-4H-pyrazol-1-yl)phenyl]foramido)methylpyridin-1-ium bromide (5e). Physical data: Yield: 96.53%; black solid; mp: 211 °C; ¹H NMR: (400 MHz, DMSO-d₆), δ_H: 9.36–9.38 (t, 1H, *J* = 5.60, 5.72, 11.32 Hz, H—12), 9.00–9.02 (d, 2H, *J* = 6.32 Hz, H—16, 17), 8.07–8.09 (d, 2H, *J* = 6.28 Hz, H—15, 18), 7.98–8.01 (d, 2H, *J* = 8.64 Hz, H—6, 10), 7.88–7.90 (d, 2H, *J* = 8.68 Hz, H—7, 9), 7.59–7.61 (d, 1H, *J* = 7.44 Hz, H—22), 7.47–7.54 (m, 3H, H—23, 24, 25), 5.97 (s, 2H, H—19), 4.76–4.77 (d, 2H, *J* = 5.32 Hz, H—13), 2.13 (s, 3H, H—1); ¹³C NMR: (400 MHz, DMSO-d₆): 166.71, 162.79, 161.17, 145.19, 133.77, 132.09, 131.98, 130.61, 129.58, 128.96, 128.84, 128.67, 126.42, 119.38, 117.37, 61.11, 42.83, 17.81; IR: (FT-IR, cm⁻¹): 3212, 3034, 1711, 1638; MS: (HR-ESI⁺), [M-Br]⁺, *m/z*: calcd.: 433.1425, found: 433.1441.

2.1.2.6. 1-[(3-Chlorophenyl)methyl]-4-([4-(3-methyl-5-oxo-4H-pyrazol-1-yl)phenyl]foramido)methylpyridin-1-ium bromide (5f). Physical data: Yield: 21.31%; black solid; mp: 228 °C; ¹H NMR: (400 MHz, DMSO-d₆), δ_H: 9.30–9.33 (t, 1H, *J* = 5.60, 5.83, 11.43 Hz, H—12), 9.09–9.11 (d, 2H, *J* = 6.6 Hz, H—16, 17), 8.05–8.07 (d, 2H, *J* = 6.44 Hz, H—14, 18), 7.96–7.98 (d, 2H, *J* = 8.72 Hz, H—6, 10), 7.87–7.89 (d, 2H, *J* = 8.76 Hz, H—7, 9), 7.69 (s, 1H, H—21), 7.47–7.52 (t, 3H, *J* = 13.62, 6.22, 19.84 Hz, H—23, 24, 25), 5.81 (s, 2H, H—19), 4.73–4.74 (d, 2H, *J* = 5.40 Hz, H—13), 2.13 (s, 3H, H—1); ¹³C NMR: (400 MHz, DMSO-d₆): 166.69, 160.90, 144.89, 137.00, 134.16, 131.62, 129.83, 129.31, 128.83, 128.05, 126.60, 62.31, 42.84, 14.62; IR: (FT-IR, cm⁻¹): 3213, 3035, 1710, 1639; MS: (HR-ESI⁺), [M-Br]⁺, *m/z*: calcd.: 433.1425, found: 433.1430.

2.1.2.7. 1-[(2-Bromophenyl)methyl]-4-([4-(3-methyl-5-oxo-4H-pyrazol-1-yl)phenyl]foramido)methylpyridin-1-ium bromide (5g). Physical data: Yield: 94.2%; black solid; mp: 204 °C; ¹H NMR: (400 MHz, DMSO-d₆), δ_H: 9.53–9.37 (t, 1H, *J* = 5.60, 5.83, 11.43 Hz, H—12), 8.98–9.00 (d, 2H, *J* = 6.52 Hz, H—16, 17), 8.07–8.09 (d, 2H, *J* = 6.40 Hz, H—15, 18), 7.87–8.00 (m, 4H, H—6, 7, 9, 10), 7.76–7.78 (d, 1H, *J* = 7.60 Hz, H—25), 7.49–7.53 (t, 1H, *J* = 7.06, 7.40, 14.46 Hz, H—22), 7.36–7.44 (m, 2H, H—23, 24), 5.94 (s, 2H, H—19),

4.76–4.78 (d, 2H, $J=5.44$, H—13), 2.13 (s, 3H, H—1); ^{13}C NMR: (400 MHz, DMSO- d_6): 166.71, 162.77, 161.21, 145.24, 133.91, 133.56, 132.04, 131.98, 129.18, 128.96, 128.84, 126.41, 123.98, 63.17, 42.84, 14.62; IR: (FT-IR, cm^{-1}): 3217, 3034, 1711, 1638; MS: (HR-ESI $^+$) [M-Br] $^+$, m/z : calcd.: 477.0920, found: 477.0928.

2.1.2.8. 1-([3-Bromophenyl)methyl]-4-([4-(3-methyl-5-oxo-4H-pyrazol-1-yl)phenyl]foramido) methylpyridin-1-ium bromide (5h). Physical data: Yield: 17.73%; dark grey solid; mp: 230 °C; ^1H NMR: (400 MHz, DMSO- d_6), δ_{H} : 9.30–9.33 (t, 1H, $J=5.60$, 5.72, 11.32 Hz, H—12), 9.09–9.10 (d, 2H, $J=6.4$ Hz, H—16, 17), 8.05–8.07 (d, 2H, $J=6.32$ Hz, H—15, 18), 7.96–7.98 (d, 2H, $J=8.60$ Hz, H—6, 10), 7.87–7.89 (d, 2H, $J=8.64$ Hz, H—7, 9), 7.83 (s, 1H, H—21), 7.63–7.65 (d, 1H, $J=8.00$ Hz, H—23), 7.52–7.54 (d, 1H, $J=7.76$ Hz, H—25), 7.39–7.54 (t, 1H, $J=7.74$, 7.90, 15.64 Hz, H—24), 5.80 (s, 2H, H—19), 4.73–4.74 (s, 2H, $J=5.36$ Hz, H—13), 2.13 (s, 3H, H—1); ^{13}C NMR: (400 MHz, DMSO- d_6): 166.69, 160.89, 144.88, 137.24, 132.74, 132.15, 131.86, 128.83, 128.43, 126.60, 122.72, 62.26, 42.84; IR: (FT-IR, cm^{-1}): 3216, 3035, 1711, 1638; MS: (HR-ESI $^+$), [M-Br] $^+$, m/z : calcd.: 477.0920, found: 477.0940.

2.1.2.9. 1-([4-Bromophenyl)methyl]-4-([4-(3-methyl-5-oxo-4H-pyrazol-1-yl)phenyl]foramido) methylpyridin-1-ium bromide (5i). Physical data: Yield: 97.42%; black solid; mp: 190 °C; ^1H NMR: (400 MHz, DMSO- d_6), δ_{H} : 9.33–9.36 (t, 1H, $J=5.95$, 11.90 Hz, H—12), 9.08–9.10 (d, 2H, $J=6.80$ Hz, H—16, 17), 8.06–8.07 (d, 2H, $J=6.64$ Hz, H—15, 18), 7.95–7.99 (m, 2H, H—6, 10), 7.89–7.87 (d, 2H, $J=8.88$ Hz, H—7, 9), 7.65–7.68 (d, 2H, $J=8.40$ Hz, H—22, 24), 7.48–7.50 (d, 2H, $J=8.44$ Hz, H—21, 25), 5.81 (s, 2H, H—8), 4.72–4.74 (d, 2H, $J=5.52$ Hz, H—13), 2.13 (s, 3H, H—1); ^{13}C NMR: (400 MHz, DMSO- d_6): 166.67, 162.77, 160.85, 144.84, 134.11, 132.64, 131.58, 128.96, 128.84, 126.56, 123.34, 62.32, 42.80; IR: (FT-IR, cm^{-1}): 3217, 3034, 1715, 1638; MS: (HR-ESI $^+$), [M-Br] $^+$, m/z : calcd.: 477.0920, found: 477.0943.

2.1.2.10 4-([4-(3-Methyl-5-oxo-4H-pyrazol-1-yl)phenyl]foramido)methyl-1-(2-methylphenyl)-pyridin-1-ium bromide (5j). Physical data: Yield: 21.75%; light grey solid; mp: 194 °C; ^1H NMR: (400 MHz, DMSO- d_6), δ_{H} : 9.34–9.37 (t, 1H, $J=5.60$, 5.83, 11.43 Hz, H—12), 8.93–8.95 (d, 2H, $J=6.64$ Hz, H—16, 17), 8.06–8.08 (d, 2H, $J=6.56$ Hz, H—15, 18), 7.98–8.00 (d, 2H, $J=8.80$ Hz, H—6, 10), 7.87–7.89 (d, 2H, $J=8.80$ Hz, H—7, 9), 7.20–7.37 (m, 3H, H—23, 24, 25), 7.12–7.14 (d, 1H, $J=7.52$ Hz, H—26), 5.88 (s, 2H, H—19), 4.75–4.76 (d, 2H, $J=5.40$ Hz, H—13), 2.29 (s, 3H, H—22), 2.13 (s, 3H, H—1); ^{13}C NMR: (400 MHz, DMSO- d_6): 166.70, 162.77, 160.81, 144.98, 137.38, 132.82, 131.43, 129.87, 129.57, 128.95, 128.83, 127.20, 126.49, 117.37, 61.36, 42.81, 19.23, 17.19; IR: (FT-IR, cm^{-1}): 3215, 3035, 1715, 1639; MS: (HR-ESI $^+$), [M-Br] $^+$, m/z : calcd.: 413.1972, found: 413.1968.

2.1.2.11. 4-([4-(3-Methyl-5-oxo-4H-pyrazol-1-yl)phenyl]foramido)methyl-1-(3-methylphenyl)-pyridin-1-ium bromide (5k). Physical data: Yield: 98.3%; black powder; mp: 212 °C; ^1H NMR: (400 MHz, DMSO- d_6), δ_{H} : 9.31–9.34 (t, 1H, $J=5.60$, 5.83, 11.43 Hz, H—12), 9.08–9.09 (d, 2H, $J=6.64$ Hz, H—16, 17), 8.04–8.06 (d, 2H, $J=6.52$ Hz, H—15, 18), 7.96–7.98 (d, 2H, $J=8.88$ Hz, H—6, 10), 7.87–7.89 (d, 2H, $J=8.80$ Hz, H—7, 9), 7.33–7.35 (d, 1H, $J=5.24$ Hz, H—21), 7.29–7.31 (t, 2H, $J=2.35$, 7.40, 9.75 Hz, H—24, 25), 7.23–7.24 (d, 1H, $J=6.84$ Hz, H—26), 5.77 (s, 2H, H—19), 4.72–4.73 (d, 2H, $J=5.44$ Hz, H—13), 2.30 (s, 3H, H—23), 2.13 (s, 3H, H—1); ^{13}C NMR: (400 MHz, DMSO- d_6): 166.68, 160.68, 144.76, 139.10, 134.76, 130.46, 129.75, 129.63, 128.83, 126.52, 126.32, 63.19, 42.81,

21.38, 17.1; IR: (FT-IR, cm^{-1}): 3208, 3034, 1716, 1638; MS: (HR-ESI $^+$), [M-Br] $^+$, m/z : calcd.: 413.1972, found: 413.1973.

2.1.2.12. 4-([4-(3-Methyl-5-oxo-4H-pyrazol-1-yl)phenyl]foramido)methyl-1-(4-methylphenyl)-pyridin-1-ium bromide (5l). Physical data: Yield: 60.13%; light grey solid; mp: 230 °C; ^1H NMR: (400 MHz, DMSO- d_6), δ_{H} : 9.30–9.33 (t, 1H, $J=5.60$, 5.83, 11.43 Hz, H—12), 9.06–9.08 (d, 2H, $J=6.6$ Hz, H—167, 17), 8.03–8.05 (d, 2H, $J=6.52$ Hz, H—15, 18), 7.96–7.98 (d, 2H, $J=8.68$ Hz, H—6, 10), 7.86–7.89 (d, 2H, $J=8.76$ Hz, H—7, 9), 7.41–7.43 (d, 2H, $J=7.96$ Hz, H—21, 26) 7.24–7.26 (d, 2H, $J=7.88$ Hz, H—22, 25), 5.76 (s, 2H, H—19), 4.71–4.72 (d, 2H, $J=5.44$ Hz, H—13), 2.29 (s, 3H, H—24), 2.13 (s, 3H, H—1); ^{13}C NMR: (400 MHz, DMSO- d_6): 166.67, 160.64, 144.67, 139.89, 131.89, 130.24, 129.29, 128.82, 126.50, 63.01, 42.81, 21.21, 17.1; IR: (FT-IR, cm^{-1}): 3224, 3032, 1714, 1638; MS: (HR-ESI $^+$), [M-Br] $^+$, m/z : calcd.: 413.1972, found: 413.1974.

2.2. Ache molecular docking studies

Molecular Operating Environment (MOE) 2018.10 software package⁴¹ was employed to predict the interactions and binding modes of the novel compounds within the active site of TcAChE. The co-crystallised structure of TcAChE with donepezil (PDB accession code: 1EVE) was acquired from the Protein Data Bank (PDB)³⁸. The following protocol was employed, as previously described⁴², to simulate the orientation and binding interactions of the test compounds. Firstly, the test compounds were drawn using ChemSketch v2019.2.1 and saved as a mol files. Secondly, the enzyme structures were inspected for missing atoms, bonds and contacts. Thirdly, partial charges and hydrogens were added using MOEs' protonate 3D application. Fourthly, the ligands were assembled employing the builder module in MOE and energy minimisation (MMFF94x) was performed. Thereafter, the ligands were docked, using the MOEdock application, within the AChE active site. Finally, the retained best poses, as per their binding affinity scores, were inspected visually and analysis of the interactions within the active aromatic gorge of AChE was conducted. To determine the accuracy of this docking protocol, the co-crystallised ligand, was re-docked into the AChE active site. This procedure was repeated three times and the best ranked solution exhibited an RMSD value of less than 2.0 Å from the position of the co-crystallised ligand. The RMSD value in this case is smaller than 2.0 Å indicating that the docking protocol is capable of accurately predicting the binding orientation of the co-crystallised ligand⁴³. This protocol was thus deemed to be suitable for the docking of inhibitors into the active site model of AChE.

2.3. Pharmacological evaluation studies

2.3.1. Cholinesterase inhibition assay

A modified Ellman's method was employed to determine the ChE inhibitory activities of the synthesised compounds⁴⁴. eeAChE, eqBuChE, 5,5'-dithiobis-(2-nitrobenzoic acid) (DTNB, commonly known as Ellman's reagent), S-butrylthiocholine iodide (BTCl), acetylthiocholine iodide (ATCl) and donepezil were purchased from Sigma-Aldrich[®]. eeAChE, eqBuChE, DTNB, BTCl and ATCl were diluted with a buffer solution (tris hydrochloride (50 mM), pH 8). Each well of a 96 well plate, contained the following; 148 μL of 1.5 mM DTNB, 50 μL of either 0.22 U/ml eeAChE or 0.12 U/ml eqBuChE and 2 μL of either test compound, control (donepezil) or blank [dimethyl sulfoxide (DMSO)]. The test compounds and control were dissolved in DMSO and added to the well to yield

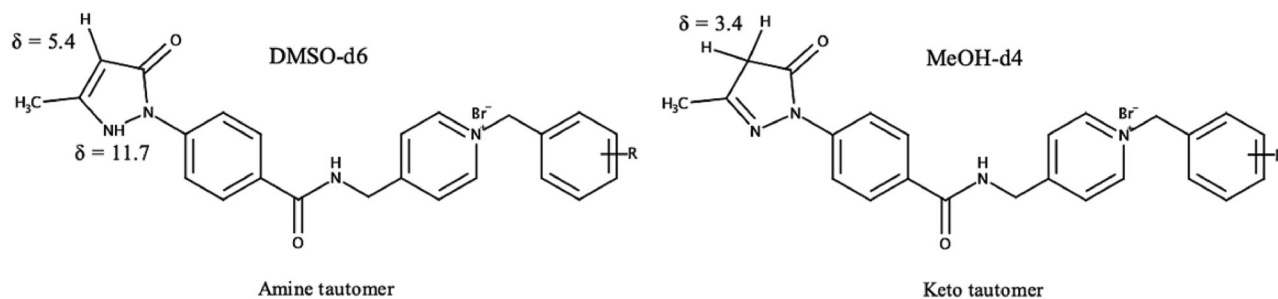


Figure 5. Two major tautomeric forms of the edaravone-*N*-benzyl pyridinium hybrid compounds and their respective ^1H NMR chemical tautomeric shifts in deuterated solvents.

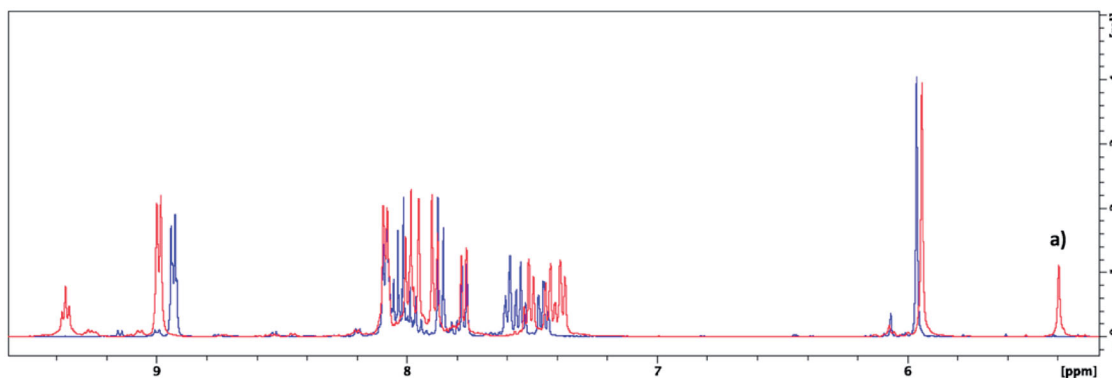


Figure 6. Overlaid ^1H NMR spectra of compound **5g** in methanol- d_4 (blue) and DMSO- d_6 (red). (a) Singlet that represents the CH-group of the amine tautomer.

found to be more stable as no peaks were present at $\delta = 5.4$ ppm and $\delta = 11.7$ ppm (Figure 6). This finding is in accordance to previous research as it has been found that the enol and keto tautomeric forms are both found within this solvent system. In addition, the keto tautomer was found to be the predominant of the two tautomeric forms in methanol⁶¹. The enol tautomer ^1H NMR peak for the CH-group at $\delta = \sim 6.2$ ppm⁶² was not present and further confirms the presence of the keto tautomer within the methanol- d_4 solvent system. The formation of the edaravone tautomers are dependent on certain solvation effects and electrostatic interactions between the solvent and molecule and further studies are to be conducted to explore the tautomeric nature of these hybrid molecules. Based on the data in this study, the keto tautomer of these hybrid molecules seems to be more stable in polar protic solvents whereas its amine tautomeric form is more stable in polar aprotic solvents. As the biological evaluations on these compounds were carried out in protic environments it is expected that the keto tautomer will be the predominant form present. The effects of the different tautomers on the biological profile of these compounds should therefore be taken into consideration for future pharmaceutical development.

The inhibitory activities of the synthesised compounds were evaluated using eeAChE (*electric eel*) and eqBuChE (*equine serum*) according to a modified method of Ellman⁴⁴. Donepezil, a known potent ChE inhibitor, was used as the reference compound for both assays. This reference compound was chosen as the structure of donepezil contains similarities to the *N*-benzyl pyridinium moiety of the synthesised compounds. Compounds **5b–5g** exhibited some of the best inhibitory activities (Table 1). These compounds have either a fluorine or chlorine substituted at various positions of the benzyl moiety and exhibited IC_{50} values between 1.2 and $4.6\ \mu\text{M}$. It can be deduced that smaller and more electronegative substitutions, such as fluorine or chlorine, in comparison to larger substitutions, such as bromine (**5h–5j**) or methyl (**5g–5i**), is

Table 1. *In silico* BBB predictions and IC_{50} values (μM) of the test compounds and controls for eeAChE, eqBuChE, and DPPH⁺.

Compound	R...	AChE	BuChE	SI AChE ^a	DPPH ⁺	BBB prediction ^b
3	–	>100	>1000	n.d.	12.5	0.108
5a	H	30	>1000	>33	22.9	0.081
5b	2-F	1.2	>1000	>83	28.8	0.068
5c	3-F	4.6	926	201	25	0.064
5d	4-F	3.6	>1000	>278	11.5	0.064
5e	2-Cl	1.9	890	468	13.8	0.060
5f	3-Cl	3.3	891	270	13.1	0.055
5g	2-Br	3.5	160	46	19	0.055
5h	3-Br	>100 μM	>1000	n.d.	13.3	0.062
5i	4-Br	11.5	>1000	>87	18.1	0.056
5j	2-CH ₃	19.9	630	32	9.5	0.056
5k	3-CH ₃	69.1	>1000	>15	27.5	0.080
5l	4-CH ₃	95.5	>1000	>11	14.5	0.077
1	–	n.d.	n.d.	n.d.	45.7	–
Donepezil ^c	–	0.006	7.14	1252	–	–
Trolox	–	n.d.	n.d.	n.d.	13.1	–
Edaravone ^d	–	–	–	–	–	–

^aAChE selectivity index = $\text{IC}_{50}(\text{eqBuChE})/\text{IC}_{50}(\text{eeAChE})$.

^bA value higher than 0.02 is predicted to cross the BBB using AlzPlatform's inter-grade cloud computing server^{49,63}.

^c IC_{50} values of donepezil reported by reference [64].

^d IC_{50} values of edaravone reported by reference [65].

n.d.: not determined.

preferred as it results in superior inhibitory activity (Table 1). The majority of the final compounds also exhibited improved activity compared to the unsubstituted benzyl moiety of **5a**.

In addition, all the compounds with substituents in the ortho position of the benzyl ring (**5b**, **5e**, **5g**, **5j**) exhibited the highest inhibitory activities when compared to their meta and para counterparts. This finding is similar to that reported in previous studies^{37,66}. The superior activity observed for **5a–5l** when compared to intermediate **3**, could be due to the increase in the length of the molecule. Molecular modelling corresponds with this observation in that **3** is too short to interact with both the PAS and CAS

of the AChE active site. This also confirms the importance of the *N*-benzyl pyridinium group for optimal AChE inhibitory activity within these compounds.

Compounds **5a–5l** also exhibited highly selective AChE inhibitory activity over BuChE (Table 1, SI:11 – >278). It can be speculated that the poor BuChE inhibitory results exhibited by all the compounds are due to the phenyl ring of edaravone and the pyridinium moiety exhibiting π – π interactions with the aromatic residues of AChE but are not able to exhibit similar interactions with BuChE's aliphatic and/or aromatic residues^{67,68}. The *N*-benzyl pyridinium moiety presents a similar structure to donepezil's benzylpyridine moiety⁶⁹. Therefore, the high selectivity of the hybrid compounds for AChE compared to BuChE was expected. Selectivity to AChE is advantageous as it has been shown to result in lower incidences of cholinergic side effects and wider therapeutic indices compared to non-selective cholinesterase inhibitors⁷⁰. Most of the hybrid compounds exhibited proficient AChE inhibitory activity when compared to previously designed, AChE acting MTDLs³⁰.

The 2,2-diphenyl-1-picrylhydrazyl (DPPH⁺) assay was employed to determine the antioxidant ability of the synthesised compounds. Trolox, a known potent antioxidant, was used as the reference compounds for this assay⁷¹. Compounds **3**, **5d–j** and **5l** (IC₅₀: 9.5–19 μ M) exhibited similar or greater antioxidant activity when compared to the control, Trolox (IC₅₀ = 13.1 μ M). In addition, these compounds retained the antioxidant activity of edaravone (IC₅₀ = 4.7 μ M)⁶⁵. Compound **5j** had the best IC₅₀ of 9.5 μ M. The rest of the compounds within the series exhibited greater antioxidant activity compared to **1**. These results correspond with previous literature in that a large lipophilic substitution on the 4-position of the phenyl ring of the edaravone moiety improves its antioxidant activity when compared to a smaller carboxylic group on the 4-position of the phenyl ring of the edaravone structure^{58,72,73}.

Potential AD therapeutic agents are required to cross the blood–brain barrier (BBB) to act in the CNS. Therefore, an *in silico* model^{49,63} was used to determine the blood–barrier permeability of the synthesised compounds. The BBB permeability prediction score represents the compounds ability to cross the BBB. A threshold score of over 0.02 is considered that the compounds are BBB permeable (BBB+) and a score below 0.02 is considered that the compounds are BBB impermeable (BBB–). The results are shown in Table 1. All the compounds exhibit scores of above 0.02 and are therefore predicted to effectively cross the BBB.

4. Conclusions

The main goal of this study was to design and synthesise a novel series of multi-target directed edaravone-*N*-benzyl pyridinium hybrid compounds that exhibit cholinesterase inhibitory activity and significant antioxidant ability. The molecular modelling results showed that these compounds should be able to form significant interactions within the PAS and CAS of the AChE active site, which in turn should lead to notable inhibitory activities. The *in vitro* cholinesterase results indicated excellent selective AChE inhibitory activity. Compounds **5b–g** demonstrated the best AChE inhibitory activity showing that smaller substitutions, e.g. fluorine and chlorine, especially in the ortho benzyl position is important for AChE inhibitory activity. Compounds **5d–j** and **5l** exhibited potent antioxidant activity that was comparable to trolox and edaravone. *In silico* blood–brain barrier evaluations predicted that all these hybrid compounds should cross the BBB. Compound **5d–g** presented as the most promising MTDL candidates against AD. These

compounds exhibited excellent selective AChE inhibitory activities (IC₅₀: 1.9–3.6 μ M), promising antioxidant abilities (IC₅₀: 11.5–19 μ M) and are predicted to cross the BBB. Further exploration of these compounds' abilities to exhibit A β inhibitory activity, neuroprotection and their pharmacokinetic- and toxicity profiles are recommended.

Acknowledgements

The authors are thankful to Prof Edith Antunes for assisting in the NMR experiments and Mr. Peter Keel for his assistance throughout this study.

Disclosure statement

No potential conflict of interest was reported by the author(s).

Funding

This work was financially supported by the University of the Western Cape and the National Research Foundation of South Africa [111811].

ORCID

Sarel F. Malan  <http://orcid.org/0000-0002-1640-6457>

Jacques Joubert  <http://orcid.org/0000-0003-0378-7091>

References

- Karantzoulis S, Galvin JE. Distinguishing Alzheimer's disease from other major forms of dementia. *Expert Rev Neurother* 2011;11:1579–91.
- Alzheimer's Association. 2019 Alzheimer's disease facts and figures. *Alzheimer's Dement* 2019;15:321–87.
- Simunkova M, Alwasel SH, Alhazza IM, et al. Management of oxidative stress and other pathologies in Alzheimer's disease. *Arch. Toxicol* 2019;93:2491–513.
- World Health Organization. Dementia [online]. 2019. Available from: <https://www.who.int/news-room/fact-sheets/detail/dementia>
- Chopra K, Misra S, Kuhad A. Current perspectives on pharmacotherapy of Alzheimer's disease. *Expert Opin Pharmacother* 2011;12:335–50.
- Selkoe DJ, Hardy J. The amyloid hypothesis of Alzheimer's disease at 25 years. *EMBO Mol Med* 2016;8:595–608.
- Hardy J, Selkoe DJ. The amyloid hypothesis of Alzheimer's disease: progress and problems on the road to therapeutics. *Science* 2002;297:353–6.
- Kung HF. The β -amyloid hypothesis in Alzheimer's disease: seeing is believing. *ACS Med Chem Lett* 2012;3:265–7.
- Pimplikar SW. Reassessing the amyloid cascade hypothesis of Alzheimer's disease. *Int J Biochem Cell Biol* 2009;41:1261–8.
- Tramutola A, Lanzillotta C, Perluigi M, Butterfield DA. Butterfield, oxidative stress, protein modification and Alzheimer disease. *Brain Res Bull* 2017;133:88–96.
- Lahiri DK, Farlow MR, Greig NH, Sambamurti K. Current drug targets for Alzheimer's disease treatment. *Drug Dev Res* 2002;56:267–81.

12. Jalili-Baleh L, Babaei E, Abdpour S, et al. A review on flavonoid-based scaffolds as multi-target-directed ligands (MTDLs) for Alzheimer's disease. *Eur J Med Chem* 2018;152:570–89.
13. Weinstock. Selectivity of cholinesterase inhibition. *CNS Drugs* 1999;12:307–23.
14. Lushchekina SV, Kots ED, Novichkova DA, et al. Role of acetylcholinesterase in β -amyloid aggregation studied by accelerated molecular dynamics. *BioNanoSci* 2017;7:396–402.
15. Belluti F, Bartolini M, Bottegoni G, et al. Benzophenone-based derivatives: a novel series of potent and selective dual inhibitors of acetylcholinesterase and acetylcholinesterase-induced beta-amyloid aggregation. *Eur J Med Chem* 2011;46:1682–93.
16. Semenov VE, Zueva IV, Mukhamedyarov MA, et al. 6-Methyluracil derivatives as bifunctional acetylcholinesterase inhibitors for the treatment of Alzheimer's disease. *ChemMedChem* 2015;10:1863–74.
17. Huang WJ, Zhang X, Chen WW. Role of oxidative stress in Alzheimer's disease. *Biomed Rep* 2016;4:519–22.
18. Cheignon C, Tomas M, Bonnefont-Rousselot D, et al. Oxidative stress and the amyloid beta peptide in Alzheimer's disease. *Redox Biol* 2018;14:450–64.
19. Poprac P, Jomova K, Simunkova M, et al. Targeting free radicals in oxidative stress-related human diseases. *Trends Pharmacol Sci* 2017;38:592–607.
20. Kell DB. Towards a unifying, systems biology understanding of large-scale cellular death and destruction caused by poorly liganded iron: Parkinson's, Huntington's, Alzheimer's, prions, bactericides, chemical toxicology and others as examples. *Arch Toxicol* 2010;84:825–89.
21. Butterfield DA. The 2013 SFRBM discovery award: selected discoveries from the butterfield laboratory of oxidative stress and its sequela in brain in cognitive disorders exemplified by Alzheimer disease and chemotherapy induced cognitive impairment. *Free Radic Biol Med* 2014;74:157–74.
22. Butterfield DA, Drake J, Pocernich C, Castegna A. Evidence of oxidative damage in Alzheimer's disease brain: central role for amyloid beta-peptide. *Trends Mol Med* 2001;7:548–54.
23. Cai Z, Zhao B, Ratka A. Oxidative stress and β -amyloid protein in Alzheimer's disease. *Neuromolecular Med* 2011;13:223–50.
24. Butterfield DA, Griffin S, Münch G, Pasinetti GM. Amyloid beta-peptide and amyloid pathology are central to the oxidative stress and inflammatory cascades under which Alzheimer's disease brain exists. *J Alzheimers Dis* 2002;4:193–201.
25. Butterfield DA, Boyd-Kimball D. Redox proteomics and amyloid β -peptide: insights into Alzheimer disease. *J Neurochem* 2019;151:459–87.
26. Singh M, Kaur M, Chadha N, Silakari O. Hybrids: a new paradigm to treat Alzheimer's disease. *Mol Divers* 2016;20:271–97.
27. Yiannopoulou KG, Papageorgiou SG. Current and future treatments for Alzheimer's disease. *Ther Adv Neurol Disord* 2013;6:19–33.
28. Briggs R, Kennelly SP, O'Neill D. Drug treatments in Alzheimer's disease. *Clin Med (Lond)* 2016;16:247–53.
29. Cavalli A, Bolognesi ML, Minarini A, et al. Multi-target-directed ligands to combat neurodegenerative diseases. *J Med Chem* 2008;51:347–72.
30. Unzeta M, Esteban G, Bolea I, et al. Multi-target directed donepezil-like ligands for Alzheimer's disease. *Front Neurosci* 2016;10:1–24.
31. Qiang X, Li Y, Yang X, et al. DL-3-n-Butylphthalide-edaravone hybrids as novel dual inhibitors of amyloid- β aggregation and monoamine oxidases with high antioxidant potency for Alzheimer's therapy. *Bioorg Med Chem Lett* 2017;27:718–22.
32. Kikuchi K, Kawahara KI, Uchikado H, et al. Potential of edaravone for neuroprotection in neurologic diseases that do not involve cerebral infarction. *Exp Ther Med* 2011;2:771–5.
33. Zhou S, Yu G, Chi L, et al. Neuroprotective effects of edaravone on cognitive deficit, oxidative stress and tau hyperphosphorylation induced by intracerebroventricular streptozotocin in rats. *Neurotoxicology* 2013;38:136–45.
34. Watanabe T, Tahara M, Todo S. The novel antioxidant edaravone: from bench to bedside. *Cardiovasc Ther* 2008;26:101–14.
35. Jiao S-S, Yao X-Q, Liu Y-H, et al. Edaravone alleviates Alzheimer's disease-type pathologies and cognitive deficits. *Proc Natl Acad Sci U S A* 2015;112:5225–30.
36. Lan JS, Zhang T, Liu Y, et al. Design, synthesis and biological activity of novel donepezil derivatives bearing N-benzyl pyridinium moiety as potent and dual binding site acetylcholinesterase inhibitors. *Eur J Med Chem* 2017;133:184–96.
37. Alipour M, Khoobi M, Foroumadi A, et al. Novel coumarin derivatives bearing N-benzyl pyridinium moiety: Potent and dual binding site acetylcholinesterase inhibitors. *Bioorg Med Chem* 2012;20:7214–22.
38. Mollazadeh M, Mohammadi-Khanaposhtani M, Zonouzi A, et al. New benzyl pyridinium derivatives bearing 2,4-dioxochroman moiety as potent agents for treatment of Alzheimer's disease: Design, synthesis, biological evaluation, and docking study. *Bioorg Chem* 2019;87:506–15.
39. Nadri H, Pirali-Hamedani M, Moradi A, et al. 5,6-Dimethoxybenzofuran-3-one derivatives: a novel series of dual acetylcholinesterase/butyrylcholinesterase inhibitors bearing benzyl pyridinium moiety. *DARU J Pharm Sci* 2013;21:1–9.
40. Baharloo F, Moslemin MH, Nadri H, et al. Benzofuran-derived benzylpyridinium bromides as potent acetylcholinesterase inhibitors. *Eur J Med Chem* 2015;93:196–201.
41. Chemical computing group. Molecular Operating Environment (MOE) Version 2015.10 [Online]. 2015. Available from: <http://www.chemcomp.com>
42. Denya I, Malan SF, Enogieru AB, et al. Design, synthesis and evaluation of indole derivatives as multifunctional agents against Alzheimer's disease. *Medchemcomm* 2018;9:357–70.
43. Binda C, Li M, Hubalek F, et al. Insights into the mode of inhibition of human mitochondrial monoamine oxidase B from high-resolution crystal structures. *Proc Natl Acad Sci U S A* 2003;100:9750–5.
44. Ellman GL, Courtney KD, Andres V, Feather-Stone RM. A new and rapid colorimetric determination of acetylcholinesterase activity. *Biochem Pharmacol* 1961;7:88–95.
45. Timm M, Saaby L, Moesby L, Hansen EW. Considerations regarding use of solvents in in vitro cell based assays. *Cytotechnology* 2013;65:887–94.
46. Cotellet N, Bernier JL, Catteau JP, et al. Antioxidant properties of hydroxy-flavones. *Free Radic Biol Med* 1996;20:35–43.
47. Brand-Williams W, Cuvelier ME, Berset C, Leben-Wiss W. Use of a free radical method to evaluate antioxidant activity. *Technol Food Sci Technol* 1995;28:25–30.

48. Teponnou GAK, Joubert J, Malan SF. Tacrine, trolox and tryptoline as lead compounds for the design and synthesis of multi-target agents for Alzheimer's Disease Therapy. *Open Med Chem J* 2017;11:24–37.
49. Liu H, Wang L, Lv M, et al. AlzPlatform: an Alzheimer's disease domain-specific chemogenomics knowledgebase for polypharmacology and target identification research. *J Chem Inf Model* 2014;54:1050–60.
50. Xie X-Q, Chen J-Z, Billings EM. 3D structural model of the G-protein-coupled cannabinoid CB2 receptor. *Proteins* 2003;53:307–19.
51. Vladimir VN. The nature of statistical learning theory. 2nd ed. New York (NY): Springer; 1995. Chapter 5.6.
52. Zhao YH, Abraham MH, Ibrahim A, et al. Predicting penetration across the blood-brain barrier from simple descriptors and fragmentation schemes. *J Chem Inf Model* 2007;47:170–5.
53. De Ferrari GV, Canales MA, Shin I, et al. A structural motif of acetylcholinesterase that promotes amyloid beta-peptide fibril formation. *Biochemistry* 2001;40:10447–57.
54. Leong SW, Abas F, Lam KW, et al. 2-Benzoyl-6-benzylidencyclohexanone analogs as potent dual inhibitors of acetylcholinesterase and butyrylcholinesterase. *Bioorg Med Chem* 2016;24:3742–51.
55. Castro A, Martinez A. Peripheral and dual binding site acetylcholinesterase inhibitors: implications in treatment of Alzheimer's disease. *Mini Rev Med Chem* 2001;1:267–72.
56. Pakaski M, Rakonczay Z, Kasa P. Reversible and irreversible acetylcholinesterase inhibitors cause changes in neuronal amyloid precursor protein processing and protein kinase C level in vitro. *Neurochem Int* 2001;38:219–26.
57. Tougu V. Acetylcholinesterase: mechanism of catalysis and inhibition. *Curr Med Chem CNS Agents* 2001;1:155–70.
58. Watanabe K, Tanaka M, Yuki S, et al. How is edaravone effective against acute ischemic stroke and amyotrophic lateral sclerosis? *J Clin Biochem Nutr* 2018;62:20–38.
59. Pal S, Mareddy J, Devi NS. High speed synthesis of pyrazolones using microwave-assisted neat reaction technology. *J Brazilian Chem Soc* 2008;19:1207–14.
60. Ruiz DL, Albesa AG, Ponzinibbio A, et al. Solvent effects on tautomeric equilibria in β -ketonitriles: NMR and theoretical studies. *J Phys Org Chem* 2010;23:985–94.
61. Ohara K, Fujii A, Ichimura Y, et al. Kinetic study of radical-scavenging and vitamin E-regenerating actions of edaravone (3-Methyl-1-phenyl-2-pyrazolin-5-one). *Bullet Chem Soc Jpn* 2006;79:421–6.
62. Erturk AG, Omerustaoglu H. Synthesis and cytotoxic evaluation of some substituted 5-pyrazolones and their urea derivatives. *Molecules* 2020;25:900–20.
63. Cbligand.org. Blood–Brain Barrier Predictor [online]. 2009. Available from: <https://www.cbligand.org/BBB/predictor.php>
64. Sugimoto H, Iimura Y, Yamanishi Y, Yamatsu K. Synthesis and anti-acetylcholinesterase activity of 1-benzyl-4-[(5,6-dimethoxy-1-indanon-2-yl)methyl]piperidine hydrochloride (E2020) and related compounds'. *Bioorg Med Chem Lett* 1992;2:871–6.
65. Tokumaru O, Shuto Y, Ogata K, et al. Dose-dependency of multiple free radical-scavenging activity of edaravone. *J Surg Res* 2018;228:147–53.
66. Mostofi M, Mohammadi Ziarani G, Mahdavi M, et al. Synthesis and structure-activity relationship study of benzofuran-based chalconoids bearing benzylpyridinium moiety as potent acetylcholinesterase inhibitors. *Eur J Med Chem* 2015;103:361–9.
67. Darvesh S, Hopkins DA, Geula C. Neurobiology of butyrylcholinesterase. *Nat Rev Neurosci* 2003;4:131–8.
68. Darvesh S, Reid GA, Martin E. E. Biochemical and histochemical comparison of cholinesterases in normal and Alzheimer brain tissues. *Curr Alzheimer Res* 2010;7:386–400.
69. Harel M, Sussman JL, Krejci E, et al. Conversion of acetylcholinesterase to butyrylcholinesterase: modeling and mutagenesis. *Proc Natl Acad Sci U S A* 1992;89:10827–31.
70. Liston DR, Nielsen JA, Villalobos A, et al. Pharmacology of selective acetylcholinesterase inhibitors: implications for use in Alzheimer's disease. *Eur J Pharmacol* 2004;486:9–17.
71. Barclay LRC, Locke SJ, MacNeil JM. Autoxidation in micelles. Synergism of vitamin C with lipid-soluble vitamin E and water-soluble Trolox. *Can J Chem* 1985;63:366–74.
72. Watanabe K, Morinaka Y, Iseki K, et al. Structure-activity relationship of 3-methyl-1-phenyl-2-pyrazolin-5-one (edaravone). *Redox Rep* 2003;8:151–5.
73. Queiroz AN, Mendes APS, Leal MS, et al. Tautomerism and radical-scavenging activity of edaravone by DFT methods. *J Comput Theor Nanosci* 2010;7:153–6.